Nonlinear mechanisms for multistability in microring lasers

Guohui Yuan* and Zhuoran Wang
School of Optoelectronic Information, University of Electronic Science and Technology of China, No. 4, Section 2, North Jianshe Road, Chengdu, 610054, Sichuan Province, People's Republic of China
(Received 27 July 2015; published 26 October 2015)

We explore the effects of nonlinear mechanisms, i.e., carrier density pulsation, carrier heating, and spectral hole burning on mode multistability in microring lasers (MRLs) both theoretically and numerically. Expressions for achieving mode multistable operation are derived and analyzed. We find that nonlinear mechanisms play an important role in mode multistability. We verify the theoretical results by numerical simulations, and find that spectral hole burning is more effective than carrier density pulsation and carrier heating in increasing the number of multistable modes in MRLs. The results also show that a decrease in the ring radius will result in a reduction in the number of multistable modes.

DOI: 10.1103/PhysRevA.92.043833 PACS number(s): 42.55.Sa, 42.65.Pc, 42.55.Px

I. INTRODUCTION

Optical memory, logic, and switch are of great importance in optical communication and signal processing systems [1]. Ring or disk lasers [2–5] have attracted considerable recent interest as one of the candidates owing to their advantages of high speed, robustness, small size, low power consumption, and integratability with a silicon platform [6,7]. Mode multistability, a recently observed and demonstrated unique feature of ring lasers, offers them the significant advantage of high capacity due to the coexistence of direction bistability and wavelength bistability or multistability [8–12]. Therefore, mode multistable microring lasers with four or more stable states are expected and are more promising to achieve even lower power consumption, higher integration densities, and more new functions.

Mode multistability in ring lasers occurs as a result of strong coupling between competing longitudinal modes through nonlinear mechanisms such as carrier density pulsation (CDP), carrier heating (CH), and spectral hole burning (SHB) [13]. The number of stable modes supported by a microring laser is naturally important since the more stable modes there are, the higher the capacity, the lower the power consumption, and the higher the integration density available. The number of stable modes depends on the size of the ring laser [14].

Although it was found that the combined effects from CDP, CH, and SHB lead to mode multistability in microring lasers [13], the role of each nonlinear mechanism is still unclear. More importantly, the effects of the nonlinear mechanisms on the number of stable modes supported by a mode multistable microring laser are also unknown. To clarify these issues is particularly meaningful for the realization of all optical high-capacity multibit memory and tunable laser technologies. Because CDP, CH, and SHB have different origins, time constants, and linewidth enhancement factors [15,16], they are expected to make different contributions to nonlinear coupling between modes and have different effects on mode multistability as well as the number of stable modes in microring lasers.

In this manuscript, we derive conditions required for mode multistability in microring lasers based on a nonlinear multimode model with CDP, CH, and SHB considered. Through the analysis of the conditions which reveal the relation between multistable modes supported in the laser and nonlinear mechanisms, we study the effects of CDP, CH, and SHB on mode multistability and especially on the number of stable modes which can be supported in the microring laser. Numerical simulations of two microring lasers with different dimensions using different CDP, CH, and SHB parameters are present to verify the theoretical results.

This paper is organized as follows: In Sec. II, we begin with a brief introduction of the theoretical model and then derive the conditions which relate the number of multistable modes with device and material parameters. Section III gives the theoretical analysis and numerical simulation results of the effects of CDP, CH, and SHB on mode multistability. Finally, we conclude our work in Sec. IV.

II. THEORY

The electric field $\varepsilon_a(z,t)$ for mode a in a multistable microring laser is expressed in terms of the complex, slowly varying electric field for mode a, E_a as

$$\varepsilon_a(z,t) = E_a(t)\exp(ik_a z)\exp(-i\omega_a t) + \text{c.c.}, \tag{1}$$

where z is the field propagation direction with counterclockwise (CCW) as positive z direction and clockwise (CW) as negative z direction, $k_a = \omega_a n_0/c$ for z direction, and $k_a = -\omega_a n_0/c$ for negative z direction, respectively, with ω_a for the optical frequency of mode a.

The dynamics of mode a is described by Eq. (2) below with two terms on the right-hand side (RHS) representing the linear effect and nonlinear coupling between modal fields, respectively:

$$\frac{dE_a}{dt} = \left\{0.5v_g\Gamma\left[g_a + \Delta N\frac{dg}{dN}(1-i\alpha_N) - \frac{1}{\Gamma v_g \tau_p}\right] - i\Delta\omega_a^{\text{dis}}\right\}E_a(t) + i0.5v_g\frac{\omega_a}{cn_0}\Gamma\sum_{bcd}\chi^3_{bcd}E_b(t) \times E_c^*(t)E_d(t)\zeta_{abcd} + F_a(t), \tag{2}$$

*yuanguohui@uestc.edu.cn

where v_g accounts for group velocity, Γ is the confinement factor, g_a represents material gain of mode a, dg/dN accounts for differential gain coefficient, α_N is the linewidth enhancement factor for carrier density pulsation, τ_p represents photon lifetime, $\Delta\omega_a^{\rm dis}$ is the total frequency shift of lasing mode frequency from the cold grid frequency, and n_0 accounts for the effective mode index. Equation (2) considers the effect of the carrier density beating which arises from beating of different existing modes. The nonlinear gain saturation effects are described by the nonlinear susceptibility derived based on the density matrix method. χ^3_{bcd} represents the combined third-order material susceptibility for the interaction between modes b, c, and d [14]. It originates from the process that the beating of modes c and d leads to modulation of the carrier distribution which interacts with mode b to generate a polarization at $\omega_b - \omega_c + \omega_d$. χ^3_{bcd} has three components contributed from CDP, CH, and SHB,

$$\chi^3_{bcd} = \chi^{\rm CDP}_{bcd} + \chi^{\rm SHB}_{bcd} + \chi^{\rm CH}_{bcd}, \tag{3}$$

$$\chi^{\rm CDP}_{bcd} = -\frac{2\varepsilon_0 n_0 n_g}{\hbar\omega_{pk}}\varepsilon_{\rm CDP}\eta^{\rm CDP}_{cd}(\alpha_{\rm CDP}+i)\frac{1}{\left(1-i\Omega\tau_{\rm CDP}\eta^{\rm CDP}_{cd}\right)\left(1-i\Omega\tau_{\rm SHB}\eta^{\rm SHB}_{cd}\right)}\chi^{1\prime\prime}_{pk}, \tag{4}$$

$$\chi^{\rm CH}_{bcd} = -\frac{2\varepsilon_0 n_0 n_g}{\hbar\omega_{pk}}\varepsilon_{\rm CH}\eta^{\rm CH}_{cd}(\alpha_{\rm CH}+i)\frac{1}{\left(1-i\Omega\tau_{\rm CH}\eta^{\rm CH}_{cd}\right)\left(1-i\Omega\tau_{\rm SHB}\eta^{\rm SHB}_{cd}\right)}\chi^{1\prime\prime}_{pk}, \tag{5}$$

$$\chi^{\rm SHB}_{bcd} = -\frac{2\varepsilon_0 n n_g}{\hbar\omega_{pk}}\varepsilon_{\rm SHB}\eta^{\rm SHB}_{cd}\frac{i}{\left(1-i\Omega\tau_{\rm SHB}\eta^{\rm SHB}_{cd}\right)[1-i(\omega_a-\omega_c)\tau_{dp}/2]}\chi^{1\prime\prime}_{pk}, \tag{6}$$

where ε_0 is permittivity of free space, χ^x_{bcd} in Eq. (3) accounts for nonlinear material susceptibility, ε_x is the nonlinear coefficient, α_x is the linewidth enhancement factor, τ_x is the time constant, and η^X_{cd} is the diffusion coefficient between modes c and d, where x refers to the nonlinear mechanisms CDP, CH, and SHB, respectively. $\Omega = \omega_d - \omega_c$ represents the beat frequency between modes c and d. τ_{dp} is the dipole relaxation time. $\chi^{\rm CDP}_{bcd}$, $\chi^{\rm CH}_{bcd}$, and $\chi^{\rm SHB}_{bcd}$ derived based on density matrix method all depend on the imaginary part of χ^1_{pk} ($\chi^{1\prime\prime}_{pk}$) which is the linear material susceptibility near the material gain peak [15]. The imaginary part of χ is related to gain g through $g = -\frac{\omega}{cn}{\rm Im}(\chi) = -\frac{\omega}{cn}\chi''$.

ζ_{abcd} accounts for spatial overlap of longitudinal mode distributions of modes a, b, c, and d with $\zeta_{abcd} = \frac{1}{L}\int_0^L \exp[i(k_a - k_b + k_c - k_d)z]dz$. ζ_{abcd} would be very small for integration over the length of many wavelengths unless the resonant coupling condition, i.e., $k_a - k_b + k_c - k_d = 0$ is satisfied. F_a is the spontaneous emission Langevin noise term. Since backscattering only weakly couples the pair of counterpropagating modes with the same cavity resonance frequency and does not have a noticeable effect on the mode multistability, it is not included in this model.

The deviation of the carrier density from its threshold value is denoted by ΔN which can be described by

$$\frac{d\Delta N}{dt} = \frac{I - I_{th}}{eV_c} - \frac{\Delta N}{\tau_N} - \frac{2\varepsilon_0 n_g n_0}{\hbar\omega_{pk}}v_g\sum_a g_a|E_a|^2, \tag{7}$$

where I accounts for the injection current, I_{th} for the threshold current, e for the elementary charge, V_c for the volume of the active region containing carriers, τ_N for differential carrier lifetime, n_g for group index, and ω_{pk} for frequency of the linear gain peak. The static carrier density change due to the intensity of modes, i.e., beating of the same modes, is considered in Eq. (7).

Assuming the laser is biased above threshold current with unidirectional mode operation, we refer to the lasing established wavelength which is the closest to the material gain peak as wavelength L and one of the bistable or multistable wavelengths as wavelengths M. Due to the direction bistability of the device, the lasing mode could be either in the CCW direction with lasing modes L_1 and M_1, or in the CW direction with lasing modes L_2 and M_2 as illustrated in Fig. 1.

We approximate the linear material gain as parabolic around ω_{pk} with gain peak equal to g_{pk}. The linear gain for mode a is given by $g_a = g_{pk}[1 - (\omega_a - \omega_{pk})^2/{\Delta\omega_{HG}}^2]$ where $\Delta\omega_{HG}$ accounts for the half width of the gain bandwidth. The lasing wavelength L is assumed to be the closest one to the linear material gain peak with angular frequency $\omega_L = \omega_{pk} + l\Delta\omega$ ($l = 0, \pm1, \ldots$) where $\Delta\omega$ is the free spectral range (FSR). The bistable or multistable wavelength M is assumed to be farther away from the linear gain peak than wavelength L with angular frequency $\omega_M = \omega_{pk} + m\Delta\omega$ ($m = \pm1, \pm2, \ldots$, and $|m| > |l|$).

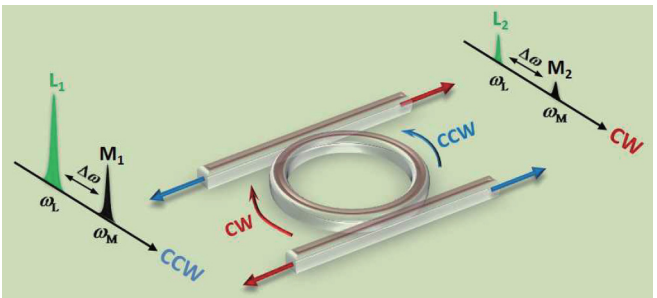

FIG. 1. (Color online) Illustration of modes L_1, M_1, L_2, and M_2 in both directions of a microring laser.

As demonstrated in Ref. [13], mode multistability can be achieved if the following conditions are satisfied:

$$\frac{g_L + \Delta N \frac{dg}{dN} - \frac{1}{\Gamma v_g \tau_p}}{\chi^{3''}_{LLL}} > \frac{g_M + \Delta N \frac{dg}{dN} - \frac{1}{\Gamma v_g \tau_p}}{\chi^{3''}_{MLL} + \chi^{3''}_{LLM}} > 0, \tag{8}$$

$$0 < \frac{g_L + \Delta N \frac{dg}{dN} - \frac{1}{\Gamma v_g \tau_p}}{\chi^{3''}_{LMM} + \chi^{3''}_{MML}} < \frac{g_M + \Delta N \frac{dg}{dN} - \frac{1}{\Gamma v_g \tau_p}}{\chi^{3''}_{MMM}}. \tag{9}$$

Here each of wavelengths L and M has a mode degeneracy of two including CCW and CW directions, i.e., modes L_1, L_2, M_1, and M_2, which means that two multistable states share the same wavelength. If conditions described by Ineqs. (8) and (9) are satisfied, the laser is mode multistable with at least four multistable modes considering the coexistence of wavelength bi/multistablity and direction bistability.

As indicated by Inequalities (Ineqs.) (8) and (9), the coupling and saturation between resonant traveling modes through nonlinear mechanisms such as CDP, CH, and SHB play important roles in mode multistability in microring lasers.

In order to gain a deeper understanding of mode multistability, we derive two new inequalities by substituting the steady-state solutions to Ineqs. (8) and (9).

The steady-state solutions are derived as

$$0 = \frac{I - I_{th}}{eV_c} - \frac{\Delta \bar{N}}{\tau_N} - \frac{2\varepsilon_0 n_g n_0}{\hbar \omega_{pk}} v_g \sum_a g_a \bar{S}_a, \tag{10}$$

$$0 = \Gamma v_g \left[g_L + \Delta \bar{N} \frac{dg}{dN} - \frac{1}{\Gamma v_g \tau_p} - \frac{\omega_{pk}}{cn} \chi^{3''}_{LLL} \bar{S}_L - \frac{\omega_{pk}}{cn} \left(\chi^{3''}_{LMM} + \chi^{3''}_{MML} \right) \bar{S}_M \right] \bar{S}_L, \tag{11}$$

$$0 = \Gamma v_g \left[g_M + \Delta \bar{N} \frac{dg}{dN} - \frac{1}{\Gamma v_g \tau_p} - \frac{\omega_{pk}}{cn} \chi^{3''}_{MMM} \bar{S}_M - \frac{\omega_{pk}}{cn} \left(\chi^{3''}_{MLL} + \chi^{3''}_{LLM} \right) \bar{S}_L \right] \bar{S}_M. \tag{12}$$

In terms of Ineq. (8), where wavelength L is lasing and remains stable, i.e., the intensity of wavelength M, $\bar{S}_M = 0$, we find the steady-state solutions as

$$\bar{S}_M = 0, \tag{13}$$

$$\bar{S}_L = \frac{\tau_N \frac{dg_L}{dN} \frac{I - I_{th}}{eV_c} + g_L - \frac{1}{\Gamma v_g \tau_p}}{\tau_N \frac{dg_L}{dN} \frac{2\varepsilon_0 n_g n}{\hbar \omega_{pk}} v_g g_L + \frac{\omega_{pk}}{cn} \chi^{3''}_{LLL}}, \tag{14}$$

$$g_L + \Delta \bar{N} \frac{dg}{dN} - \frac{1}{\Gamma v_g \tau_p} = \frac{\omega_{pk}}{cn} \chi^{3''}_{LLL} \bar{S}_L = \frac{\omega_{pk}}{cn} \chi^{3''}_{LLL} \frac{\tau_N \frac{dg_L}{dN} \frac{I - I_{th}}{eV_c} + g_L - \frac{1}{\Gamma v_g \tau_p}}{\tau_N \frac{dg_L}{dN} \frac{2\varepsilon_0 n_g n}{\hbar \omega_{pk}} v_g g_L + \frac{\omega_{pk}}{cn} \chi^{3''}_{LLL}}. \tag{15}$$

By substituting Eqs. (13)–(15) into Ineq. (8), we obtain

$$\frac{\frac{\omega_{pk}}{cn} \left(\chi^{3''}_{MLL} + \chi^{3''}_{LLM} - \chi^{3''}_{LLL} \right) \bar{S}_L + g_{pk} (m^2 - l^2) \left(\frac{\Delta \omega}{\Delta \omega_{HG}} \right)^2}{\chi^{3''}_{MLL} + \chi^{3''}_{LLM}} > 0 \tag{16}$$

Because $\chi^{3''}_{MLL} + \chi^{3''}_{LLM} > 0$ holds for most frequencies except for the frequencies ranging from a few gigahertz less than zero to zero, we can readily assume that $\chi^{3''}_{MLL} + \chi^{3''}_{LLM} > 0$ and change Ineq. (16) to the following:

$$\begin{aligned} (m^2 - l^2) \left(\frac{\Delta \omega}{\Delta \omega_{HG}} \right)^2 &> \frac{\omega_{pk}}{g_{pk} cn} \left(\chi^{3''}_{LLL} - \chi^{3''}_{MLL} - \chi^{3''}_{LLM} \right) \bar{S}_L \\ &= \frac{-\chi^{3''}_{LLL} + \chi^{3''}_{MLL} + \chi^{3''}_{LLM}}{\chi^{1''}_{pk}} \frac{\tau_N \frac{dg_L}{dN} \frac{I - I_{th}}{eV_c} + g_L - \frac{1}{\Gamma v_g \tau_p}}{\tau_N \frac{dg_L}{dN} \frac{2\varepsilon_0 n_g n}{\hbar \omega_{pk}} v_g g_L + \frac{\omega_{pk}}{cn} \chi^{3''}_{LLL}}. \end{aligned} \tag{17}$$

By recalling that $\frac{\omega_{pk}}{cn} \chi^{3''}_{LLL} \ll \tau_N \frac{dg_L}{dN} \frac{2\varepsilon_0 n_g n}{\hbar \omega_{pk}} v_g g_L$, we finally have

$$\begin{aligned} m^2 - l^2 &> \left(\frac{\Delta \omega_{HG}}{\Delta \omega} \right)^2 \frac{-\chi^{3''}_{LLL} + \chi^{3''}_{MLL} + \chi^{3''}_{LLM}}{\chi^{1''}_{pk}} \bar{S}_L \\ &\approx \left(\frac{\Delta \omega_{HG}}{\Delta \omega} \right)^2 \frac{-\chi^{3''}_{LLL} + \chi^{3''}_{MLL} + \chi^{3''}_{LLM}}{\chi^{1''}_{pk}} \frac{\tau_N \frac{dg_L}{dN} \frac{I - I_{th}}{eV_c} + g_L - \frac{1}{\Gamma v_g \tau_p}}{\tau_N \frac{dg_L}{dN} \frac{2\varepsilon_0 n_g n}{\hbar \omega_{pk}} v_g g_L}. \end{aligned} \tag{18}$$

Similarly, by substituting the steady-state solutions to Ineq. (9) where wavelength M is lasing and remains stable, i.e., the intensity of wavelength L, $\bar{S}_L = 0$, we obtain

$$m^2 - l^2 < \left(\frac{\Delta\omega_{HG}}{\Delta\omega}\right)^2 \frac{\chi^{3''}_{MMM} - \chi^{3''}_{LMM} - \chi^{3''}_{MML}}{\chi^{1''}_{pk}} \bar{S}_M$$
$$\approx \left(\frac{\Delta\omega_{HG}}{\Delta\omega}\right)^2 \frac{\chi^{3''}_{MMM} - \chi^{3''}_{LMM} - \chi^{3''}_{MML}}{\chi^{1''}_{pk}} \frac{\tau_N \frac{dg_M}{dN} \frac{I-I_{th}}{eV_c} + g_M - \frac{1}{\Gamma v_g \tau_p}}{\tau_N \frac{dg_M}{dN} \frac{2\varepsilon_0 n_g n}{\hbar\omega_{pk}} v_g g_M}. \quad (19)$$

Inequalities (18) and (19) not only give the conditions required for achieving mode multistable operation in microring lasers but also reveal the relation between the number of multistable mode and device and material parameters. It indicates that if Ineq. (18) holds but Ineq. (19) does not, wavelength L would be the only stable wavelength, and modes L_1 and L_2 would be the only stable modes considering mode degeneracy. On the contrary, if Ineq. (19) holds but Ineq. (18) does not, wavelength M in both directions will be the only stable wavelength, and M_1 and M_2 would be the only stable modes considering mode degeneracy. If both Ineqs. (18) and (19) hold, mode multistability with at least four multistable modes can be realized.

III. ANALYTICAL ANALYSIS AND NUMERICAL RESULTS

A. Analytical analysis

As indicated by Ineqs. (18) and (19), mode multistability of a microring lasers is closely related to device and material parameters. Furthermore, how many multistable modes a microring laser can support also relies on these parameters. Both Ineqs. (18) and (19) have to hold in order to achieve mode multistability.

In order to study the role of nonlinear mechanisms in mode multistability, we rewrite Ineqs. (18) and (19) as

$$\frac{-\chi^{3''}_{LLL} + \chi^{3''}_{MLL} + \chi^{3''}_{LLM}}{\chi^{1''}_{pk}} < (m^2 - l^2)\left(\frac{\Delta\omega}{\Delta\omega_{HG}}\right)^2 \frac{\tau_N \frac{dg_L}{dN} \frac{2\varepsilon_0 n_g n}{\hbar\omega_{pk}} v_g g_L}{\tau_N \frac{dg_L}{dN} \frac{I-I_{th}}{eV_c} + g_L - \frac{1}{\Gamma v_g \tau_p}}, \quad (20)$$

$$\frac{\chi^{3''}_{MMM} - \chi^{3''}_{LMM} - \chi^{3''}_{MML}}{\chi^{1''}_{pk}} > (m^2 - l^2)\left(\frac{\Delta\omega}{\Delta\omega_{HG}}\right)^2 \frac{\tau_N \frac{dg_M}{dN} \frac{2\varepsilon_0 n_g n}{\hbar\omega_{pk}} v_g g_M}{\tau_N \frac{dg_M}{dN} \frac{I-I_{th}}{eV_c} + g_M - \frac{1}{\Gamma v_g \tau_p}}. \quad (21)$$

The left-hand side (LHS) of Ineq. (20) is given by $(-\chi^{3''}_{LLL} + \chi^{3''}_{MLL} + \chi^{3''}_{LLM})/\chi^{1''}_{pk}$, and the LHS of Ineq. (21) is given by $(\chi^{3''}_{MMM} - \chi^{3''}_{LMM} - \chi^{3''}_{MML})/\chi^{1''}_{pk}$. Both $(-\chi^{3''}_{LLL} + \chi^{3''}_{MLL} + \chi^{3''}_{LLM})/\chi^{1''}_{pk}$ and $(\chi^{3''}_{MMM} - \chi^{3''}_{LMM} - \chi^{3''}_{MML})/\chi^{1''}_{pk}$ are related to the total nonlinear gain with respect to wavelength L and M, correspondingly [13]. They have three different contributions which come from three different nonlinear mechanisms, i.e., CDP, CH, and SHB. Inequalities (20) and (21) show that nonlinear mechanisms are important for mode multistability in a microring laser since $(-\chi^{3''}_{LLL} + \chi^{3''}_{MLL} + \chi^{3''}_{LLM})/\chi^{1''}_{pk}$ has to be less than the RHS of Ineq. (20) and $(\chi^{3''}_{MMM} - \chi^{3''}_{LMM} - \chi^{3''}_{MML})/\chi^{1''}_{pk}$ has to be larger than the RHS of Ineq. (21) in order to achieve mode multistability.

Because the strength of the nonlinear mechanisms depends on the frequency difference of the modes, the values of both $(-\chi^{3''}_{LLL} + \chi^{3''}_{MLL} + \chi^{3''}_{LLM})/\chi^{1''}_{pk}$ and $(\chi^{3''}_{MMM} - \chi^{3''}_{LMM} - \chi^{3''}_{MML})/\chi^{1''}_{pk}$ rely on the frequency difference $\omega_M - \omega_L$. Figures 2(a) and 2(b) show $(-\chi^{3''}_{LLL} + \chi^{3''}_{MLL} + \chi^{3''}_{LLM})/\chi^{1''}_{pk}$ and $(\chi^{3''}_{MMM} - \chi^{3''}_{LMM} - \chi^{3''}_{MML})/\chi^{1''}_{pk}$ as a function of the angular frequency difference $\omega_M - \omega_L$ which equals $(m - l)\Delta\omega$ by definition.

As illustrated by Figs. 2(a) and 2(b), the solid line gives the joint effect of the three different nonlinear mechanisms. The dashed line represents the contribution from CDP, the dotted line corresponds to that from CH, and the dash-dotted line is for SHB. Figures 2(a) and 2(b) show that the asymmetry of $(-\chi^{3''}_{LLL} + \chi^{3''}_{MLL} + \chi^{3''}_{LLM})/\chi^{1''}_{pk}$ and $(\chi^{3''}_{MMM} - \chi^{3''}_{LMM} - \chi^{3''}_{MML})/\chi^{1''}_{pk}$ are due to asymmetric CDP and CH. Because CDP, CH, and SHB have different time constants, $(-\chi^{3''}_{LLL} + \chi^{3''}_{MLL} + \chi^{3''}_{LLM})/\chi^{1''}_{pk}$ and $(\chi^{3''}_{MMM} - \chi^{3''}_{LMM} - \chi^{3''}_{MML})/\chi^{1''}_{pk}$ are dominated by different nonlinear effects in different frequency ranges. As shown by Figs. 2(a) and 2(b), CDP plays a dominant role when the frequency difference is less than 100 GHz. As the frequency difference increases to above 100 GHz, CH and SHB become the dominant mechanism with which effects from CDP decrease rapidly towards a negligible level.

In order to further understand the effects of different nonlinear mechanisms on $(-\chi^{3''}_{LLL} + \chi^{3''}_{MLL} + \chi^{3''}_{LLM})/\chi^{1''}_{pk}$ and $(\chi^{3''}_{MMM} - \chi^{3''}_{LMM} - \chi^{3''}_{MML})/\chi^{1''}_{pk}$ as well as mode multistability, we study the dependence of $(-\chi^{3''}_{LLL} + \chi^{3''}_{MLL} + \chi^{3''}_{LLM})/\chi^{1''}_{pk}$ and $(\chi^{3''}_{MMM} - \chi^{3''}_{LMM} - \chi^{3''}_{MML})/\chi^{1''}_{pk}$ on CDP, CH, and SHB. Figure 3 gives the values of $(-\chi^{3''}_{LLL} + \chi^{3''}_{MLL} + \chi^{3''}_{LLM})/\chi^{1''}_{pk}$ and $(\chi^{3''}_{MMM} - \chi^{3''}_{LMM} - \chi^{3''}_{MML})/\chi^{1''}_{pk}$ for different CDP [Fig. 3(a)], CH [Fig. 3(b)], and SHB [Fig. 3(c)] contributions as a function of the angular frequency difference $\omega_M - \omega_L$. The contribution from each nonlinear mechanism is increased from half to twice of the present values which are $1 \times 10^{-21}\,\mathrm{m}^3$ for $\varepsilon_{\mathrm{CDP}}$, $5.5 \times 10^{-23}\,\mathrm{m}^3$ for $\varepsilon_{\mathrm{CH}}$, and $3.5 \times 10^{-23}\,\mathrm{m}^3$ for $\varepsilon_{\mathrm{SHB}}$ with arrows pointing in the increasing direction in Fig. 3. The main parameters used for Figs. 2 and 3 are listed in Table I.

Figure 3(a) shows that as the contribution from CDP increases, $(-\chi^{3''}_{LLL} + \chi^{3''}_{MLL} + \chi^{3''}_{LLM})/\chi^{1''}_{pk}$ and $(\chi^{3''}_{MMM} - \chi^{3''}_{LMM} - \chi^{3''}_{MML})/\chi^{1''}_{pk}$ increase for negative frequency differences, whereas $(-\chi^{3''}_{LLL} + \chi^{3''}_{MLL} + \chi^{3''}_{LLM})/\chi^{1''}_{pk}$ and $(\chi^{3''}_{MMM} - \chi^{3''}_{LMM} - \chi^{3''}_{MML})/\chi^{1''}_{pk}$ decrease for positive frequency differences. As the contribution from CH increases, illustrated by Fig. 3(b), $(-\chi^{3''}_{LLL} + \chi^{3''}_{MLL} + \chi^{3''}_{LLM})/\chi^{1''}_{pk}$ increases for

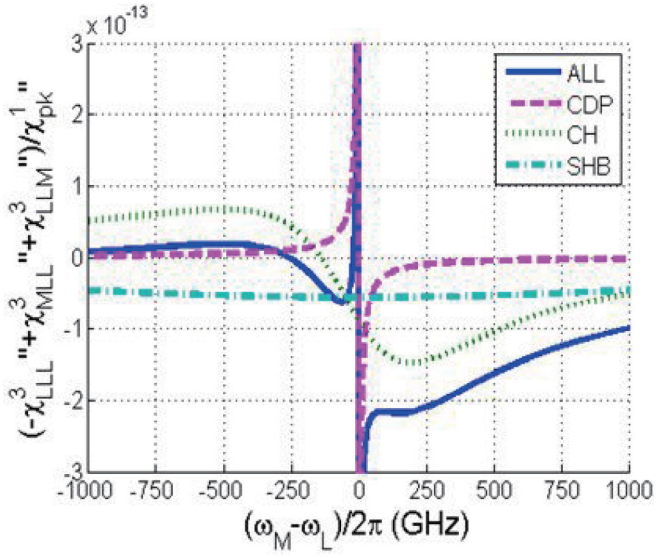

(a)

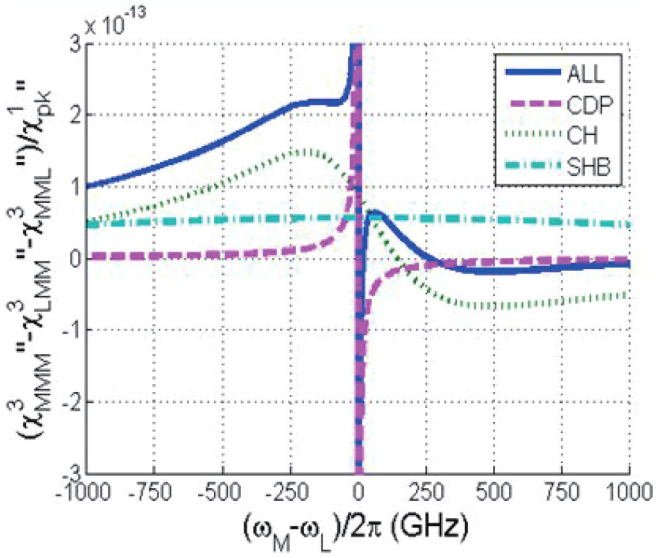

(b)

FIG. 2. (Color online) Variations of $(-\chi^{3\prime\prime}_{LLL}+\chi^{3\prime\prime}_{MLL}+\chi^{3\prime\prime}_{LLM})/\chi^{1\prime\prime}_{pk}$ (a) and $(\chi^{3\prime\prime}_{MMM}-\chi^{3\prime\prime}_{LMM}-\chi^{3\prime\prime}_{MML})/\chi^{1\prime\prime}_{pk}$ (b) with the frequency difference $\omega_M-\omega_L$ due to nonlinear effects (ALL) including contributions from CDP, CH, and SHB.

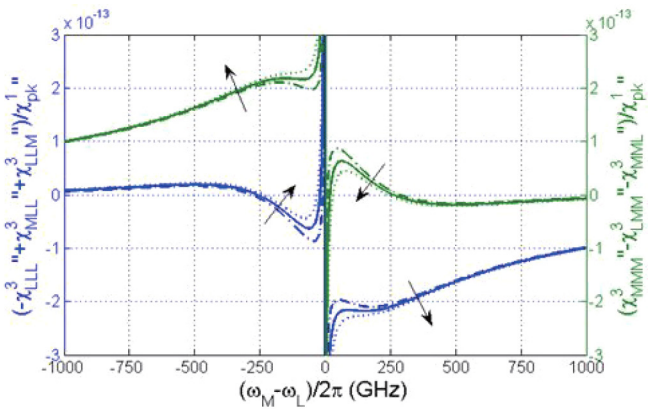

(a)

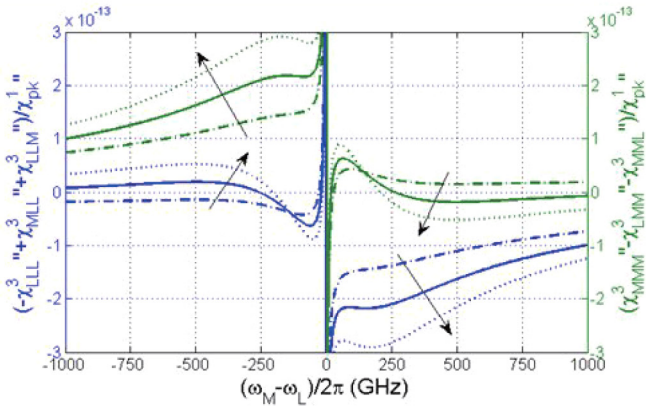

(b)

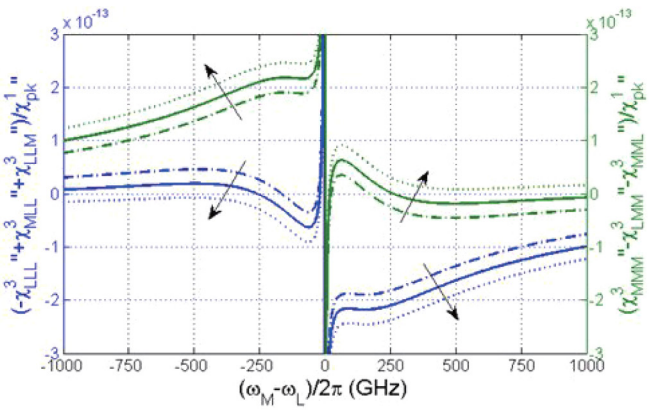

(c)

FIG. 3. (Color online) Variations of $(-\chi^{3\prime\prime}_{LLL}+\chi^{3\prime\prime}_{MLL}+\chi^{3\prime\prime}_{LLM})/\chi^{1\prime\prime}_{pk}$ and $(\chi^{3\prime\prime}_{MMM}-\chi^{3\prime\prime}_{LMM}-\chi^{3\prime\prime}_{MML})/\chi^{1\prime\prime}_{pk}$ as functions of the frequency difference $\omega_M-\omega_L$ with CDP (a), CH (b), and SHB (c) increased from 0.5 to 1.5 times the present values which are $1\times10^{-21}\,\mathrm{m}^3$ for $\varepsilon_{\mathrm{CDP}}$, $5.5\times10^{-23}\,\mathrm{m}^3$ for $\varepsilon_{\mathrm{CH}}$, and $3.5\times10^{-23}\,\mathrm{m}^3$ for $\varepsilon_{\mathrm{SHB}}$ in the arrow direction.

frequency differences less than –130 GHz and decreases for frequency differences larger than –130 GHz, whereas $(\chi^{3\prime\prime}_{MMM}-\chi^{3\prime\prime}_{LMM}-\chi^{3\prime\prime}_{MML})/\chi^{1\prime\prime}_{pk}$ increases for frequency differences less than 130 GHz and decreases for frequency difference larger than 130 GHz. Figure 3(c) shows that as the contribution from SHB increases, $(-\chi^{3\prime\prime}_{LLL}+\chi^{3\prime\prime}_{MLL}+\chi^{3\prime\prime}_{LLM})/\chi^{1\prime\prime}_{pk}$ decreases, whereas $(\chi^{3\prime\prime}_{MMM}-\chi^{3\prime\prime}_{LMM}-\chi^{3\prime\prime}_{MML})/\chi^{1\prime\prime}_{pk}$ increases for both negative and positive frequency differences.

Inequalities (20) and (21) show that $(-\chi^{3\prime\prime}_{LLL}+\chi^{3\prime\prime}_{MLL}+\chi^{3\prime\prime}_{LLM})/\chi^{1\prime\prime}_{pk}$ has to be less than the RHS of Ineq. (20) so that wavelength L is stable and $(\chi^{3\prime\prime}_{MMM}-\chi^{3\prime\prime}_{LMM}-\chi^{3\prime\prime}_{MML})/\chi^{1\prime\prime}_{pk}$ has to be larger than the RHS of Ineq. (21) so that wavelength M is stable. Therefore, the frequency difference range in which both wavelength L and wavelength M are stable relies on CDP, CH, and SHB as shown by Fig. 3.

As indicated by Ineqs. (20) and (21), increasing the value of $(-\chi^{3\prime\prime}_{LLL}+\chi^{3\prime\prime}_{MLL}+\chi^{3\prime\prime}_{LLM})/\chi^{1\prime\prime}_{pk}$ may lead to instability of wavelength L while decreasing the value of $(\chi^{3\prime\prime}_{MMM}-\chi^{3\prime\prime}_{LMM}-\chi^{3\prime\prime}_{MML})/\chi^{1\prime\prime}_{pk}$ may result in instability of wavelength M.

TABLE I. Main parameters.

Symbol	Description	Value
Γ	Confinement factor for all wells	0.1
λ_0	Wavelength at material gain center	1.56×10^{-6} m
n	Refractive index	3.2
n_g	Group index	3.6
N_{tr}	Carrier density at transparency	1.7×10^{24} m^{-3}
$\Delta\omega_{HG}$	Half width of the gain bandwidth	3.7×10^{13} rad/s
dg/dN	Differential gain	1.2×10^{-19} m^2
I_{th}	Threshold current	Variable
I	Bias current	$3\ I_{th}$
τ_p	Photon lifetime	Variable
τ_e	Carrier lifetime	3.14×10^{-9} s
$\alpha_{\rm CDP}$	Linewidth enhancement factor for CDP	5
$\alpha_{\rm CH}$	Linewidth enhancement factor for CH	2
$\tau_{\rm CDP}$	Time constants for CDP	0.5×10^{-9} s
$\tau_{\rm CH}$	Time constants for CH	0.5×10^{-12} s
$\tau_{\rm SHB}$	Time constants for SHB	0.05×10^{-12} s
$\varepsilon_{\rm CDP}$	Nonlinear coefficient for CDP	1×10^{-21} m^3
$\varepsilon_{\rm CH}$	Nonlinear coefficient for CH	5.5×10^{-23} m^3
$\varepsilon_{\rm SHB}$	Nonlinear coefficient for SHB	3.5×10^{-23} m^3

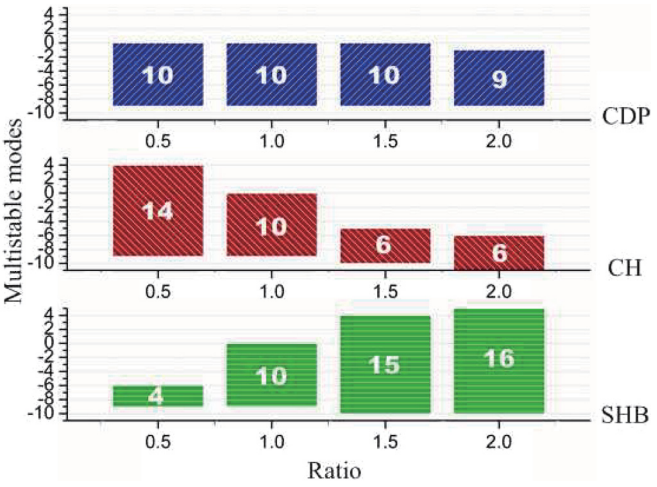

FIG. 4. (Color online) Variation of the number of multistable modes as the ratio for the nonlinear gain coefficients $\varepsilon_{\rm CDP}$, $\varepsilon_{\rm CH}$, and $\varepsilon_{\rm SHB}$ increases from 0.5 to 2 times their initial values which are 1×10^{-21} m^3 for CDP, 5.5×10^{-23} m^3 for CH, and 3.5×10^{-23} m^3 for SHB, respectively, for a microring laser with a ring radius of 100 μm.

Figure 3(a) shows that increasing the contribution from CDP may lead to a reduction in the frequency difference range in which wavelength L is stable and an increase in the frequency difference range in which wavelength M is stable for negative frequency differences, and an increase in the frequency difference range in which wavelength L is stable and a reduction in the frequency difference range in which wavelength M is stable for positive frequency differences.

Figure 3(b) illustrates that the frequency difference range in which wavelength L is stable can be reduced for frequency differences less than –130 GHz and increased for frequency differences larger than –130 GHz by increasing the contribution from CH, while the frequency difference range in which wavelength M is stable can be increased for frequency differences less than 130 GHz and reduced for frequency differences larger than 130 GHz by increasing the contribution from CH.

Figure 3(c) shows that the frequency difference range in which wavelength L is stable can be increased for both negative and positive frequency differences, while the frequency difference range in which wavelength M is stable can also be increased for both negative and positive frequency differences.

Changing any of the contributions from CDP, CH, or SHB can result in variations in $(-\chi^{3''}_{LLL} + \chi^{3''}_{MLL} + \chi^{3''}_{LLM})/\chi^{1''}_{pk}$ and $(\chi^{3''}_{MMM} - \chi^{3''}_{LMM} - \chi^{3''}_{MML})/\chi^{1''}_{pk}$, and the amount of variation depends on nonlinear mechanism and frequency difference.

Assuming initially wavelength L is the only stable wavelength, as suggested by Fig. 3, an increase in CDP and CH may lead to an increase in $(\chi^{3''}_{MMM} - \chi^{3''}_{LMM} - \chi^{3''}_{MML})/\chi^{1''}_{pk}$ for frequency differences which are mainly negative and consequent appearance of multistable wavelength M on the low-frequency (long-wavelength) side. Further increase in CDP and CH may cause wavelength L to be unstable for the original wavelength at the material gain peak and shift to the one with lower frequency (longer wavelength) due to further increase in $(-\chi^{3''}_{LLL} + \chi^{3''}_{MLL} + \chi^{3''}_{LLM})/\chi^{1''}_{pk}$. Whereas an increase in SHB will lead to a decrease in $(-\chi^{3''}_{LLL} + \chi^{3''}_{MLL} + \chi^{3''}_{LLM})/\chi^{1''}_{pk}$ as well as an increase in $(\chi^{3''}_{MMM} - \chi^{3''}_{LMM} - \chi^{3''}_{MML})/\chi^{1''}_{pk}$ for both negative and positive frequency differences and consequent appearance of multistable wavelength M on both the low- and high-frequency (long- and short-wavelength) sides without affecting the stability of wavelength L.

B. Numerical results

We simulate a microring laser based on a nonlinear multimode model described by Eqs. (2) and (7) with a total of 30 modes from both CW and CCW directions considered. The device which is assumed to be fabricated using a multiple quantum-well material system is a ridge waveguide circular laser with a straight output waveguide coupled to the ring via a directional coupler. The parameters used in the simulation, which are the same as those used in Figs. 2 and 3, are listed in Table I.

Simulated results of the multistable modes are given in Figs. 4 and 5 as the ratio for the nonlinear gain coefficients $\varepsilon_{\rm CDP}$, $\varepsilon_{\rm CH}$, and $\varepsilon_{\rm SHB}$ increases from 0.5 to 2 times their initial values which are 1×10^{-21} m^3, 5.5×10^{-23} m^3, and 3.5×10^{-23} m^3 correspondingly, for devices with ring radius of 100 and 50 μm, respectively. Threshold current, photon lifetime, carrier lifetime, and cavity round-trip time are recalculated correspondingly as the radius changes.

Figure 4 shows that as the contribution from CDP increases, the range of multistable modes for the device with a ring radius of 100 μm varies from –9 to 0 ($l = 0$, $m = -9$ to -1) to –9 to –1 ($l = -1$, $m = -9$ to -2). With increasing contribution from CH, the range of multistable modes changes from –9 to 4 ($l = 0$, $m = -9$ to -1, 1 to 4) to –11 to –6 ($l = -6$, $m = -11$ to -7). The range of multistable modes increases from –9 to –6 ($l = -6$, $m = -9$ to -7) to –10 to 5 ($l = 0$, $m = -10$ to -1, 1 to 5) with increasing contribution from SHB.

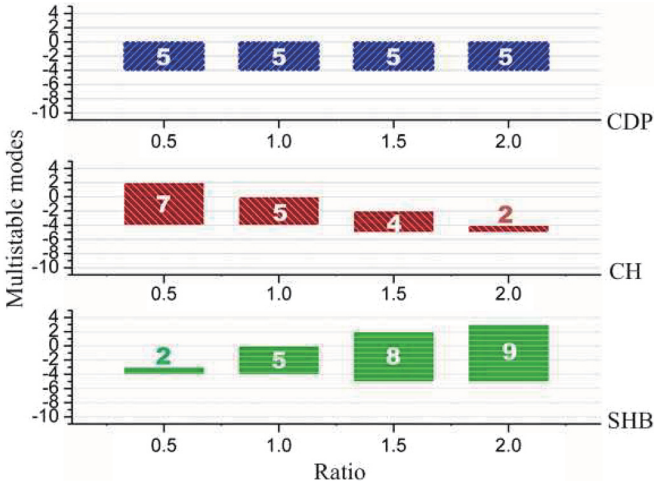

FIG. 5. (Color online) Variation of the number of multistable modes as the ratio for the nonlinear gain coefficients ε_{CDP}, ε_{CH}, and ε_{SHB} increases from 0.5 to 2 times their initial values which are 1×10^{-21} m^3 for CDP, 5.5×10^{-23} m^3 for CH, and 3.5×10^{-23} m^3 for SHB, respectively, for a mircroring laser with a ring radius of 50 μm.

Compared with Fig. 4, Fig. 5, which gives the results for the device with a ring radius of 50 μm, shows that the range of multistable modes narrows as the ring radius decreases. As illustrated in Fig. 5, the range of multistable modes remains as –4 to 0 ($l = 0$, $m = -4$ to -1) with increasing contribution for CDP. It also shows that as the nonlinear gain coefficient for CH increases, the range of multistable modes varies from –4 to 2 ($l = 0$, $m = -4$ to -1, 1 to 2) to –5 to –4 ($l = -4$, $m = -5$). The range of multistable modes increases from –4 to –3 ($l = -3$, $m = -4$) to –5 to 3 ($l = 0$, $m = -5$ to -1, 1 to 3) with increasing contribution from SHB.

The variation in the range of multistable modes caused by CDP is less than that caused by CH or SHB as shown in both Figs. 4 and 5 owing to the fact that the effect of CDP is less important than that of CH or SHB for the devices with ring radii of 50 and 100 μm whose free spectral range is larger than 100 GHz.

Figures 4 and 5 show that the multistable modes shift to those with lower frequencies (longer wavelengths) and the stable mode at the material gain peak becomes unstable with increasing contribution from CH and CDP (the latter has less noticeable effect). Because the distant mode receives less material gain than those near the material gain peak, increases in the contributions from CDP and CH may lead to a decrease in the total number of stable modes.

As the contribution from SHB increases, the range of the multistable modes expands towards both low- and high-frequency (long- and short-wavelength) sides with more distant modes becoming stable as shown in Figs. 4 and 5. However, the rate of increase slows down because distant modes receive less material gain than those near the material gain peak and they are more difficult to become stable.

IV. CONCLUSIONS

We have theoretically and numerically investigated the effects of nonlinear mechanisms, i.e., CDP, CH, and SHB, on mode multistability in microring lasers. Analytical analysis indicates that CDP dominates when the frequency difference between the established mode and competing mode is less than 100 GHz. As the frequency difference increases to above 100 GHz, CH and SHB become the dominant mechanism with which effects from CDP decrease rapidly. Asymmetric CDP and CH, and symmetric SHB result in asymmetric joint effect. An increase in the contributions from CDP and CH may lead to the appearance of multistable wavelength M on the low-frequency (long-wavelength) side. Further increase in contributions from CDP and CH may cause wavelength L to be unstable for the original wavelength at the material gain peak and shift to the one with lower frequency (longer wavelength). Whereas an increase in SHB will lead to the appearance of multistable wavelength M on both the low- and high-frequency (long- and short-wavelength) sides without affecting the stability of wavelength L.

Consistent with the analytical analysis, numerical simulation results show that the multistable modes shift to the lower-frequency (longer-wavelength) side and the initial stable mode at the material gain peak becomes unstable with increasing contributions from CH and CDP. However, further increases in the contributions from CDP and CH may result in the reduction in the total number of stable modes because the distant mode receives less material gain than those near the material gain peak. Whereas as the contribution from SHB increases, the range of the multistable modes expands towards both low- and high-frequency (long- and short-wavelength) sides with more distant stable modes. Therefore, SHB is more effective in increasing the number of multistable modes compared with CDP and CH, especially for microring lasers whose FSRs are large. The results also show that a decrease in the ring radius will result in a reduction in the number of stable modes.

ACKNOWLEDGMENTS

This work was sponsored in part by the Program for New Century Excellent Talents in University under Grant No. NCET-12-0092; the Scientific Research Foundation for the Returned Overseas Chinese Scholars of State Education Ministry under Grant No. 2012GJ002; and the National Natural Science Foundation of China under Grants No. 61575038, No. 61107088, and No. 61107061.

[1] R. S. Tucker, J. Lightwave Technol. **24**, 4655 (2006).
[2] M. Sorel, G. Giuliani, A. Scire, R. Miglierina, S. Donati, and P. J. R. Laybourn, IEEE J. Quantum Electron. **39**, 1187 (2003).
[3] M. T. Hill, H. J. S. Dorren, T. de Vries, X. J. M. Leijtens, J. H. D. Besten, B. Smalbrugge, Y. S. Oei, H. Binsma, G. D. Khoe, and M. K. Smit, Nature **432**, 206 (2004).
[4] G. Yuan and S. Yu, IEEE J. Quantum Electron. **44**, 41 (2008).

[5] Z. Wang, G. Yuan, and S. Yu, IEEE Photonics Technol. Lett. **20**, 1048 (2008).
[6] D. Liang and J. E. Bowers, Nat. Photonics **4**, 511 (2010).
[7] L. Liu, R. Kumar, K. Huybrechts, T. Spuesens, G. Roelkens, E. J. Geluk, T. D. Vries, P. Regreny, D. V. Thourhout, R. Baets, and G. Morthier, Nat. Photonics **4**, 182 (2010).
[8] C. J. Born, S. Yu, M. Sorel, and P. J. R. Laybourn, in *Proceedings of the Conference on Lasers and Electro-Optics, Baltimore, MD* (Optical Society of America, 2003), paper CWK4.
[9] Z. Wang, G. Yuan, G. Verschaffelt, J. Danckaert, and S. Yu, IEEE Photonics. Technol. Lett. **20**, 1228 (2008).
[10] A. Pérez-Serrano, J. Javaloyes, and S. Balle, Opt. Express **19**, 3284 (2011).
[11] L. Gelens, S. Beri, G. Van der Sande, G. Mezosi, M. Sorel, J. Danckaert, and G. Verschaffelt, Phys. Rev. Lett. **102**, 193904 (2009).
[12] L. Gelens, G. Van der Sande, S. Beri, and J. Danckaert, Phys. Rev. E **79**, 016213 (2009).
[13] G. Yuan and Z. Wang, Optics Express **21**, 9624 (2013).
[14] G. Yuan and Z. Wang, IEEE J. Quantum Electron. **47**, 1375 (2011).
[15] C. Born, G. Yuan, Z. Wang, and S. Yu, IEEE J. Quantum Electron. **44**, 1055 (2008).
[16] A. Godard, G. Pauliat, G. Roosen, and E. Ducloux, IEEE J. Quantum Electron. **40**, 970 (2004).